Hindawi Publishing Corporation
Journal of Nanomaterials
Volume 2012, Article ID 793084, 8 pages
doi:10.1155/2012/793084

Research Article

Raman Spectroscopy of Isotactic Polypropylene-Halloysite Nanocomposites

Elamin E. Ibrahim,[1] Dorina Magdalena Chipara,[2] Ram Thapa,[2] Karen Lozano,[3] and Mircea Chipara[2]

[1] *Department of Chemistry, The University of Texas-Pan American, Edinburg, TX 78541, USA*
[2] *Department of Physics and Geology, The University of Texas-Pan American, 1201 West University Drive, Edinburg, TX 78541, USA*
[3] *Department of Mechanical Engineering, The University of Texas-Pan American, Edinburg, TX 78541, USA*

Correspondence should be addressed to Dorina Magdalena Chipara, dchipara@utpa.edu

Received 15 June 2012; Revised 20 August 2012; Accepted 3 September 2012

Academic Editor: Steve F. A. Acquah

Raman spectroscopy investigations on nanocomposites obtained by dispersing halloysite within isotactic polypropylene are reported. A detailed analysis of the modifications of the regularity band associated to the polymeric matrix is presented. The Raman lines assigned to the polymeric matrix are broadened and weakened as the loading with halloysite is increased. The analysis of Raman lines indicates that the polymeric matrix becomes less crystalline upon the loading with halloysite and that the nanofiller is experiencing a weak dehydration upon dispersion within the polymeric matrix, probably due to the related thermal processing used to achieve the dispersion of halloysite.

1. Introduction

The dispersion of carbon nanotubes within polymeric matrices resulted in important improvements of the mechanical properties (reflected in most cases by increases of the Young modulus [1–4]) and of the thermal stability [4] of polymeric matrices. Nevertheless, the electrical and thermal conductivity of one-dimensional carbon nanostructures [5, 6] added thermal and electrical conductivity to the typically insulating polymeric matrices (especially if the concentration of the nanofiller is at or above the percolation threshold [7, 8]). For some applications, such as electrical insulators or thermal barrier materials, such modifications are adverse. Detailed investigations on isotactic polypropylene filled with other one-dimensional materials (such as single-walled carbon nanotubes, multiwalled carbon nanotubes, and carbon nanofibers) have been reported elsewhere [9–13].

Halloysite (H) is an unique nanoclay [14], with a tubular morphology and low electrical and thermal conductivity. These features incited several investigations on the physical properties of polymer-halloysite nanocomposites [14–17]. Taking into account the above-mentioned characteristics, a detailed investigation on the physical properties of isotactic polypropylene-halloysite nanocomposite has been ignited.

There are several types of halloysites, corresponding to the degree of hydration. The extremes are represented by the so-called halloysite 10 A, and by halloysite 7 A. Halloysite 10 A is characterized by a monoclinic crystalline structure (with the cell parameters $a = 5.1$ A, $b = 8.9$ A, $c = 10.25$ A, and $\beta = 100°$), with the chemical formula $Al_2Si_2O_5(OH)_4\ 2H_2O$ and the unit cell volume of about 458 A^3. Halloysite 10 A is a nanotube with diameters ranging typically between 30 to 200 nm, a wall thickness of 20 nm, and lengths ranging between 500 nm to 10,000 nm obtained by rolling together kaolinite like sheets. It is known also as endelite, hydrated halloysite, or hydrohalloysite. It is typically unstable having a strong tendency to loose water. Halloysite 7 A (with amonoclinic crystal structure and cell parameters $a = 5.14$ A, $b = 8.9$ A, $c = 14.9$ A, and $\beta = 101.9°$) has an unit volume of about 667 A^3 and it is known as the dehydrated halloysite. During the dehydration process, the distance between layers decreases from about 1 nm to 0.7 nm.

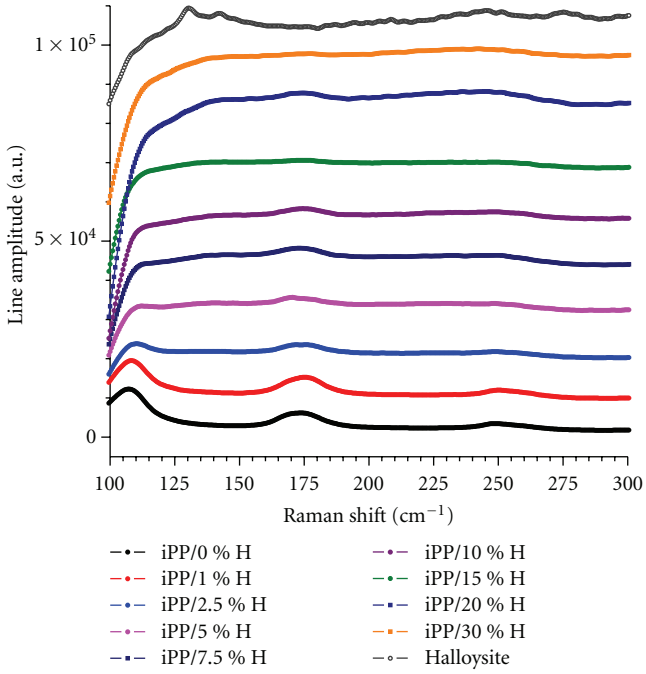

Figure 1: Raman spectra of iPPH nanocomposites for different loadings with H. From bottom to top: 0% H, 1.0% H, 2.5% H, 5.0% H, 7.5% H, 10.0% H, 15% H, 20% H, 30% H, and 100% H.

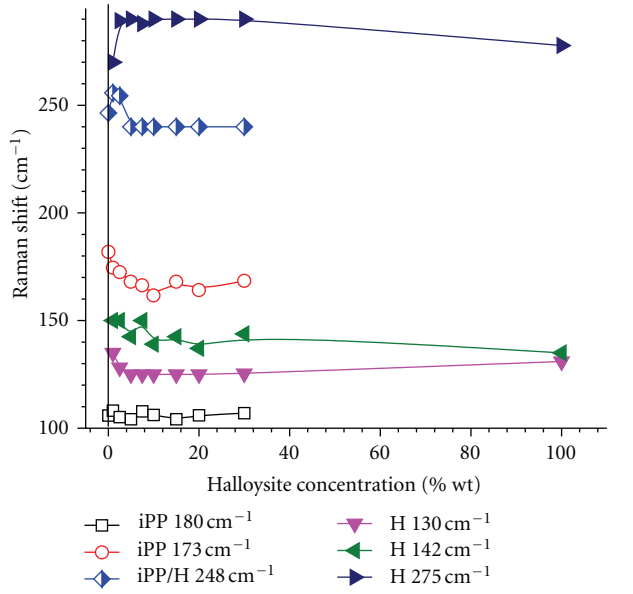

Figure 2: The effect of the loading with H on the position of Raman lines in the range from 100 to 300 cm^{-1}. iPP (or open symbols) identifies the Raman lines assigned to the matrix, and H the Raman lines due to the filler. Half-filled symbols represent overlapping lines due to iPP and H.

In halloysite, strong hydrogen interactions are responsible for the enhanced stability of hole water compared to associated water. Typically, the associated water is released at about 200°C, while the hole water survives up to about 300°C. The dehydrated halloysite is also known as metahalloysite. Several aluminosilicates (clays) have the same elemental composition $Al_2Si_2O_5(OH)_4$ as the dehydrated halloysite. Among them, the most important are (in alphabetical order) dickite, kaolinite, and nacrite. These compounds differ solely by the spatial distribution of atoms and consequently the discrimination between halloysite and any of these compounds is frequently difficult.

2. Experimental Methods

The structure and composition of naturally occurring H is expected to be intermediate between 7 A and 10 A, reflecting an $Al_2Si_2O_5(OH)_4 \cdot xH_2O$ chemical formula where x is close to zero but not precisely zero due to some crystallization water eventually retained. This derives from the fact that most dehydrated halloysite (7 A) result from the dehydration of halloysite (10 A). Isotactic polypropylene-halloysite (iPPH) nanocomposites were obtained by high-shear mixing of isotactic polypropylene (iPP; Sigma Aldrich) with various amounts of halloysite ($Al_2Si_2O_5(OH)_4 \cdot xH_2O$; from Sigma Aldrich). Kaolinite, with a close chemical structure (missing, however, the two water molecules, i.e., $Al_2Si_2O_5(OH)_4$), is sometimes also referred to as a halloysite (see, e.g., the website of Sigma Aldrich http://www.sigmaaldrich.com/catalog/product/aldrich/685445?lang=en&region=US) or as metahalloysite. The cylindrical symmetry of halloysite (H) is

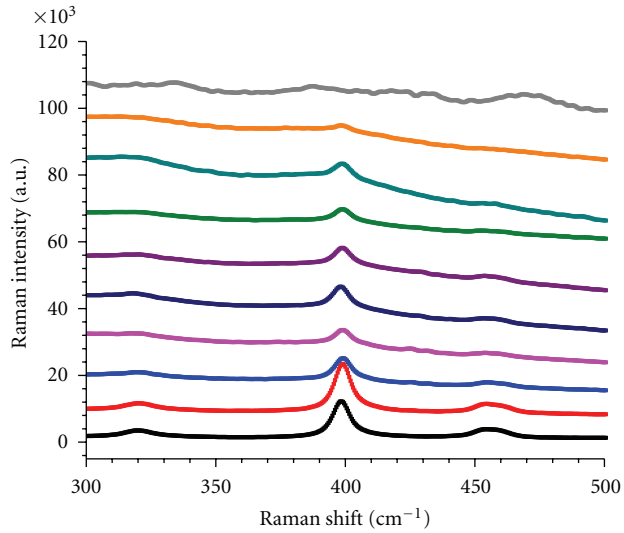

Figure 3: Raman spectra of iPPH nanocomposites for different loadings with H. From bottom to top: 0% H, 1.0% H, 2.5% H, 5.0% H, 7.5% H, 10.0% H, 15% H, 20% H, 30% H, and 100% H.

a consequence of a packing disorder. According to Sigma Aldrich, the external diameter of halloysite nanotubes is ranging between 30 and 70 nm (with an average of 50 nm), the average internal diameter is about 15 nm, and the length of halloysite is typically ranging between 1 to 3 μm. Hence, halloysite nanotubes are comparable to short-multiwalled carbon nanotubes. However, the Young modulus, the electrical conductivity, the thermal conductivity, and the thermal stability of halloysite are significantly lower than those

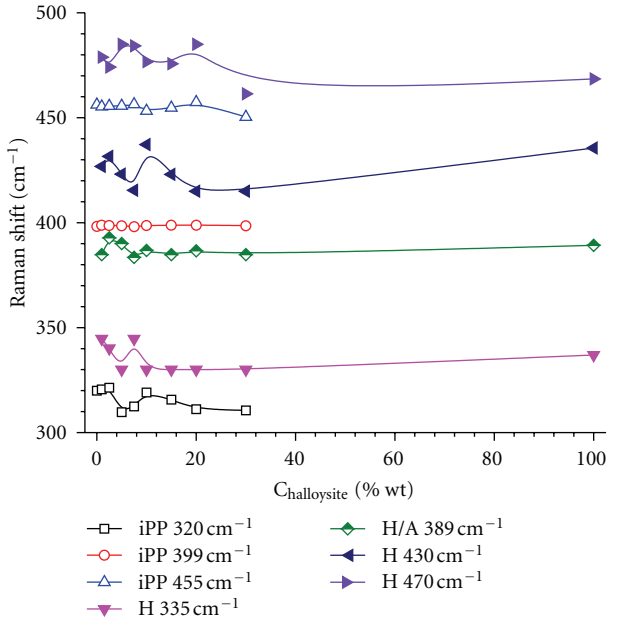

FIGURE 4: The effect of the loading with H on the position of Raman lines in the range from 300 to 500 cm^{-1}. iPP (or open symbols) identifies the Raman lines assigned to the matrix, and H the Raman lines due to the filler. Half-filled symbols represent overlapping lines due to iPP and H.

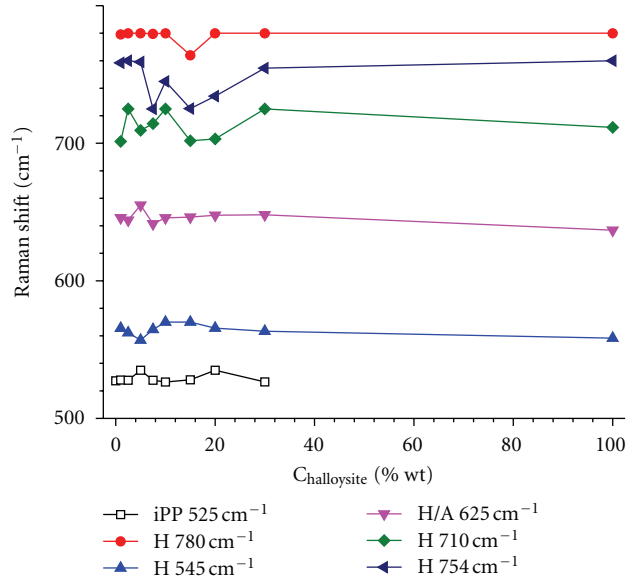

FIGURE 6: The effect of the loading with H on the position of Raman lines in the range 500 to 800 cm^{-1}. iPP (or open symbols) identifies the Raman lines assigned to the matrix, and H the Raman lines due to the filler. Half-filled symbols represent overlapping lines due to iPP, H, and A.

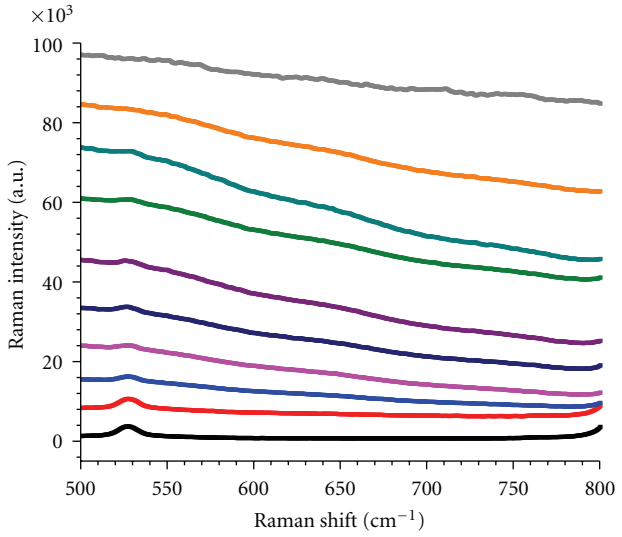

FIGURE 5: Raman spectra of iPPH nanocomposites for different loadings with H. From bottom to top: 0% H, 1.0% H, 2.5% H, 5.0% H, 7.5% H, 10.0% H, 15% H, 20% H, 30% H, and 100% H.

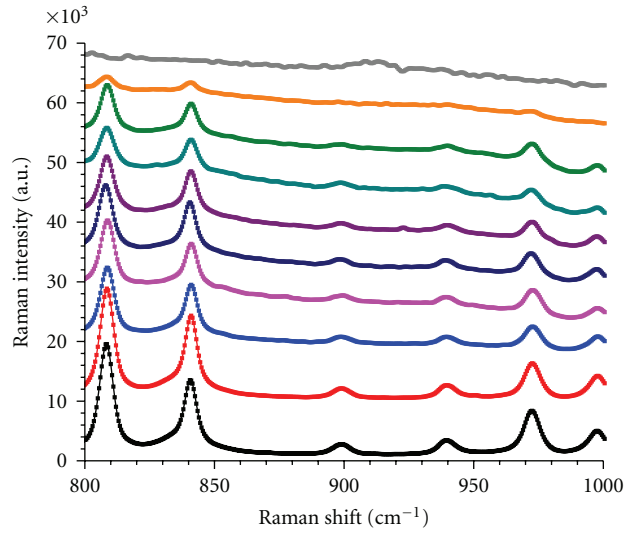

FIGURE 7: Raman spectra of iPPH nanocomposites for different loadings with H. From bottom to top: 0% H, 1.0% H, 2.5% H, 5.0% H, 7.5% H, 10.0% H, 15% H, 20% H, 30% H, and 100% H.

of multiwalled carbon nanotubes. The estimated Young modulus of halloysite is in the range from 150 to 300 GPa compared to 1000 GPa for a carbon nanotube [18]. The energy gap for halloysite is of about 9.7 eV compared to few eV (or zero) in semiconducting or metallic carbon nanotubes [18]. This classifies halloysite as an electric insulator.

The blending has been performed by utilizing a HAAKE Rheomix at 65 rpm and 180°C for 9 min followed by an additional mixing of 5 min at the same temperature and at 90 rpm. Composites loaded with various amounts of H ranging from 0% up to 30% wt. have been prepared. Raman investigations have been performed by using a Bruker Senterra dispersive confocal microscope spectrometer equipped with a 785 nm laser diode. Thermogravimetric analysis has been performed in nitrogen atmosphere by using a TA Instrument Equipment.

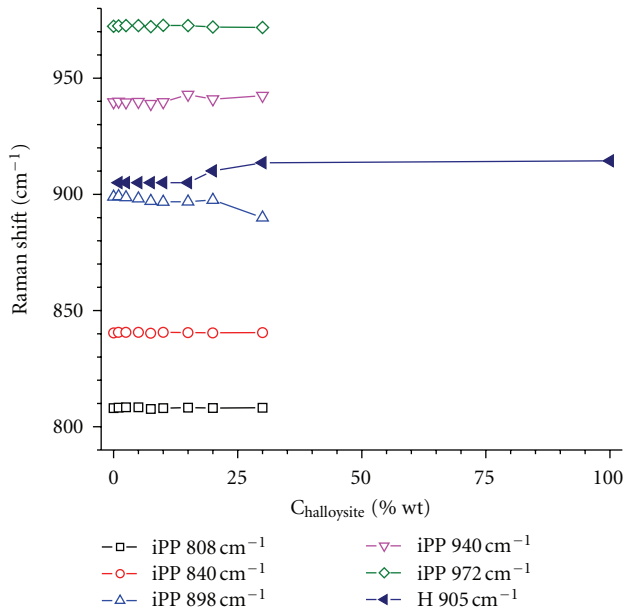

Figure 8: The effect of the loading with H on the position of Raman lines in the range from 800 to 1000 cm^{-1}. iPP (or open symbols) identifies the Raman lines assigned to the matrix, and H the Raman lines due to the filler.

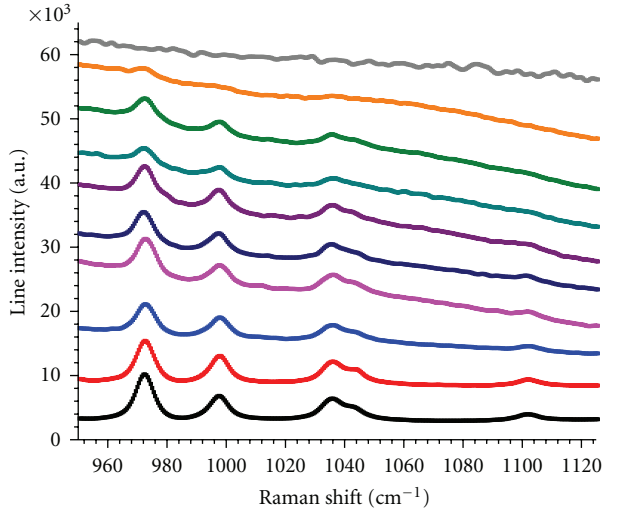

Figure 9: Raman spectra of iPPH nanocomposites for different loadings on the position of Raman lines in the range from 800 to 1000 cm^{-1}. iPP (or open symbols) identifies the Raman lines assigned to the matrix, and H the Raman lines due to the filler. Half-filled symbols represent overlapping lines due to iPP and H.

3. Experimental Results and Discussions

The Raman lines of pristine H are rather broad and weak, being superimposed on a very strong and wideband noticed at low Raman shifts (centered at about 125–150 cm^{-1} and reported as a shoulder assigned to O–Si–O bending [19]). The Raman lines of iPP are typically narrow lines. As in the case of iPP-Vapor Grown Carbon Nanofiber (VGCNF) nanocomposites [11], the addition of the filler broadens the Raman lines of the polymeric matrices up to their collapse in a very broad line. This behavior reflects the formation of an interface between the nanofiller and the polymeric chains and the final trapping of most macromolecular chains within these interfaces at loading concentrations above 20% wt.

All Raman lines have been fitted by a superposition of modified Wigner-Breit-Fano lineshapes [20]; the general expression utilized for each line was

$$I(x) = \sum_{i=1}^{N} A_i \frac{[1 + D_i(x - P_i)/W_i]^2}{1 + [(x - P_i)/W_i]^2} + B + Sx + Qx^2, \quad (1)$$

where I is the amplitude of the Raman spectral domain at a given Raman shift x (in cm^{-1}), N is the total number of lines for the spectral domain (including eventually both iPP and H lines), B is the base line correction, S is the slope correction, and Q is a quadratic correction. For each line, labeled by i, D_i is the shape deviation from a pure Lorentzian line, P_i is the corresponding Raman peak position, and W_i is the width of the line. For each spectral domain, an excellent agreement between fitted and recorded spectra was achieved, with correlation coefficients typically above 0.99. Each spectral domain involved at least 250 experimental points. The fit has been performed by using Origin Pro 8.6.

At low wavenumbers (spectral domain 100 to 300 cm^{-1}), the Raman spectrum shows the typical lines reported elsewhere (see Figure 1). The broad shoulder reported in the range from 110 to 130 cm^{-1} is easily noticed in Figure 1. Raman spectra of halloysite confirm the line located at 130.8 cm^{-1} identified as the line noticed at 134.7 cm^{-1} and assigned to the symmetric (out of the plane) bending mode of Si_2O_5 [21, 22]. Tentatively, this can be associated to the line reported at 127 cm^{-1} in the New Zeeland halloysite [23]. An intense line was noticed at 142.4 cm^{-1} and identified as the line reported at 143 cm^{-1} [23]. The origin of this line is under debate. Some authors are assigning this line to anatase impurities [19] while others are assigning this line to AlO_6 octahedron vibrations [22]. The Raman lines at 156 and 168 cm^{-1} connected to inner surface hydroxyls are absent, suggesting a low degree of hydration [21]. However, the weak lines observed at 246 (O–H–O symmetric stretch in hydrated halloysite [24]) and 276 cm^{-1} (O–H–O antisymmetric stretch in hydrated halloysite [24]) are connected to water's molecule vibrations [22].

For isotactic polypropylene, the lines located at 108 cm^{-1}, 173 cm^{-1}, and 248 cm^{-1} are easily noticed. The Raman line located at 248 cm^{-1} has been identified as the line located at 252 cm^{-1} and assigned to wagging CH_2 and bending CH groups [25, 26]. An overlap between the iPP line located at 250 cm^{-1} and the H line at 246 cm^{-1} is possible in iPPH nanocomposites.

The dependence of the Raman lines position on the loading with halloysite is shown in Figure 2. Empty symbols are connected to the polymeric matrix and solid symbols to the filler. Half-solid symbol is assigned to the overlapping signals. It is noticed that the peak located at 275 cm^{-1} is shifted towards larger Raman shift. The experimental data indicates a dehydration of the halloysite, expected during the thermal processing of the nanocomposite. It is important

to mention that in the case of halloysite, the Raman peaks were rather weak. At low concentration of halloysite, the water diffused within the polymer as moisture may hydrate weakly the filler. However, for samples containing 2.5% wt. H or a smaller amount of H, the intensity of this line is fairly low. From Figure 2 it is noticed that the position of the Raman lines of H are displaced towards smaller Raman shifts suggesting a weak dehydration of the nanofiller. This is consistent with the thermal blending and suggests a partial loss of water during the processing of the nanocomposites.

The second spectral domain, ranging between 300 and 500 cm^{-1}, includes both iPP and H lines, as shown in Figure 3. The line noticed at 335 cm^{-1} can be assigned to uncomplexed kaolinite [19] or to water in nanoclays (responsible for another Raman line typically located at 332 cm^{-1} [24]) while the weak and broad line at 389 cm^{-1} confirms the presence of anatase impurities [19]. The line at 469 cm^{-1} is tentatively assigned to Al–O/Si–O vibrations [19] and labeled as the N line.

There are three main Raman lines, which are typically assigned to iPP in this spectral domain located at about 320 cm^{-1} [26, 27], 400 cm^{-1} [26, 27], and 455 cm^{-1} [28]. The line located at about 400 cm^{-1}, assigned to the umbrella bending mode about the tertiary carbon atom [29], is the most intense one. The last line was assigned to wagging CH_2 and bending CH [28]. As noticed in Figure 4, the Raman lines of H are shifted towards lower Raman shifts as the H content is increased above 10% wt. halloysite. The position of the iPP line located at 399 cm^{-1} shows a weak shift towards larger values as the concentration of halloysite is increased. In the case of the line located at 400 cm^{-1}, it was reported that the melting is shifting this line to 402 cm^{-1} [28]. This suggests a drop of the degree of crystallinity of iPP upon loading with H. The position of the iPP line located at 455 cm^{-1} is shifted to lower values as the H content is increased. The position of the other line assigned to iPP has a complex dependence of H content showing above 10% wt. halloysite a weak shift of the line to smaller Raman shifts as the H content is increased.

Figure 5 collects the line recorded in the spectral domain from 500 cm^{-1} to 800 cm^{-1}. In this range, several Raman lines are expected. Water (in H) can contribute with a weak line located at 789 cm^{-1} [21, 22]. The line at 712 cm^{-1} is a rather weak resonance that confirms the presence of OH groups [24]. The line noticed at 754 cm^{-1} is labeled as the K line [19]. A single strong line due to iPP, located at 525 cm^{-1} and assigned to wagging CH_2, stretching C–CH_3, and rocking CH_2 [28]. The effect of the loading of iPP with H on the most important Raman lines observed in this spectral domain is shown in Figure 6. The position of the line located at 525 cm^{-1} is almost not modified by the loading with H. The position of the Raman lines assigned to H shows a complex dependence on the content of H (at low concentration of H) continuing by a weak shift towards larger values (versus H concentration) for samples containing between 10 and 30% wt. H.

Figure 7 collects the Raman lines in the spectral domain from 800 to 1000 cm^{-1}. This spectral domain is dominated by the Raman lines due to iPP. The weak Al–OH libration line [19, 24] located at 910–912 cm^{-1} and labeled as the I line is within the noise. The Raman lines originating from iPP have been observed at 808 cm^{-1} (regularity band associated with crystalline domains reflecting C–C stretching along backbone and rocking CH_3 [27, 28, 30]), 840 cm^{-1} (another regularity band due to CH_3 rocking and originating from amorphous regions [28]), 895 cm^{-1} (rocking CH_2, stretching CH_3, and bending CH [28]), and 940 cm^{-1}. The line located at 895 cm^{-1} is typically observed in melts of iPP. This confirms that the loading of iPP with halloysite drops the degree of crystallinity of the polymeric matrix and agrees with experimental data on iPP filled with VGCNFs [11, 12]. Figure 8 shows the effect of the loading with H on the position of various Raman lines. The figure includes a single line assigned to H, which is weakly shifted towards larger values. The shift is stronger for H concentrations larger than 10% wt. (At low H concentrations the shift towards larger values is slightly above the experimental errors). The iPP lines included in Figure 8 are almost independent on the concentration of H.

The Raman spectra in the range from 1000 cm^{-1} to 1100 cm^{-1} are shown in Figure 9. This spectral domain is dominated by the strong lines originating from iPP and located at 972 cm^{-1} (regularity band due to CH_3 rocking [27, 28]), 997 cm^{-1} (another regularity band that does not disappear on melting [28]), 1033 cm^{-1} (which was reported as a structural defect [28]), 1041 cm^{-1}, and 1100 cm^{-1}. Halloysite is responsible for two weak lines located at 1172 cm^{-1} and 1180 cm^{-1} assigned to Si–O units [22]. The effect of loading with H on the position of the Raman lines is shown in Figure 10. The spectra assigned to iPP are shifted towards larger Raman shifts as the content of halloysite is increased. Nevertheless, these shifts are rather weak. The dependence of the position of the halloysite limes on the content of halloysite is complex and weak. The line located at 1033 cm^{-1} indicates the enhancement of structural defects in H-doped nanocomposites. Nevertheless, the broadening of this line makes difficult an accurate estimation of the dependence of disorder degree versus the concentration of halloysite.

The isotacticity was calculated as the ratio between the area of the peak located at 809 cm^{-1} and the area of the peak located at 974 cm^{-1} [27]. Figure 11 demonstrates the drop of the isotacticity index as the polymeric matrix is loaded with H, indicating a decrease of the degree of crystallinity, consistent with other features noticed within this study.

The thermal stability of halloysite is rather poor. As can be inferred from Figure 12, the TGA data of pristine halloysite are consistent with stepwise thermal degradations centered at 250°C, 480°C, and 680°C. The first maxim is assigned to the loss of crystallization water and the second one is assigned to dehydroxilation towards kaolinite (actually metakaolin, $Al_2Si_2O_7$). Assuming that all crystallization data is lost at 300°C, the corrected structure of the pristine halloysite is $Al_2Si_2O_5(OH)_4 \cdot x\ H_2O$, where $x = 0.5$.

Raman spectra of pristine and annealed halloysite shown in Figure 13 exibit small differences, probably because the main component is the dehydrated halloysite and the recorded spectra are actually convolutions over slightly

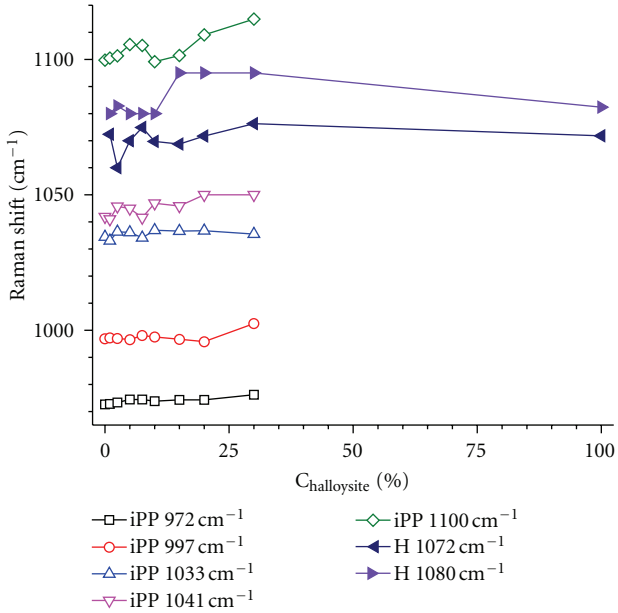

FIGURE 10: The effect of the loading with H on the position of Raman lines in the range from 1000 to 1100 cm^{-1}. iPP (or open symbols) identifies the Raman lines assigned to the matrix, and H the Raman lines due to the filler.

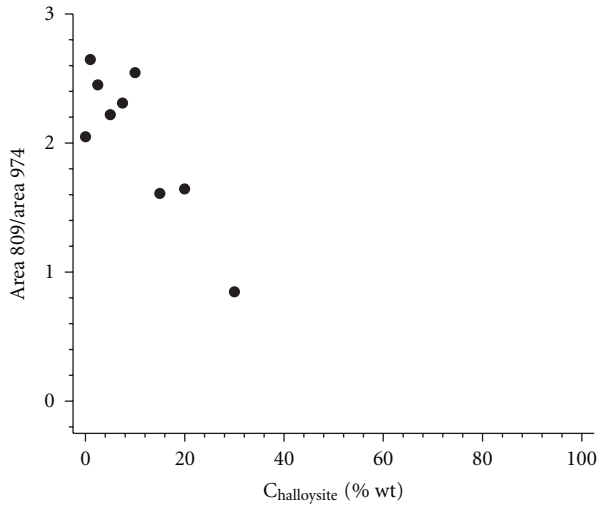

FIGURE 11: The dependence of the isotacticity index (i.e., of the ratio between the areas of the peaks located at 809 and 974 cm^{-1} on the loading with halloysite).

different structures. Figure 14 collects the Raman spectra of iPPH nanocomposites annealed at 250°C for 30 minutes. It is noticed that the annealing at 250°C (i.e., the dehydration of the halloysite) has a weak effect on the Raman spectra of iPPH nanocomposites.

4. Conclusions

Raman spectroscopy investigations on nanocomposites obtained by dispersing halloysite within iPP are reported.

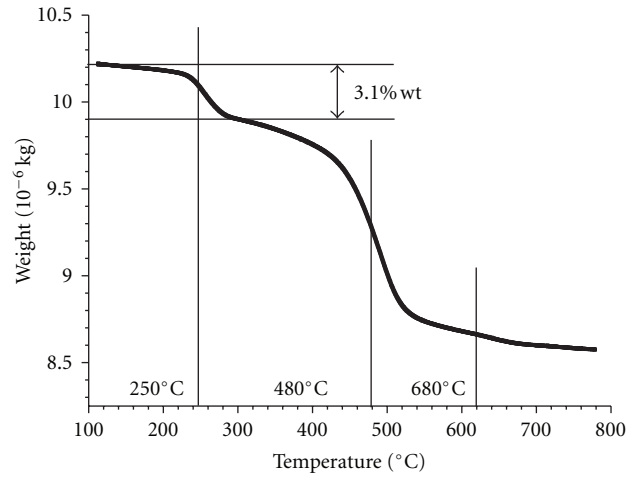

FIGURE 12: TGA data of pristine halloysite showing the main thermal degradation processes.

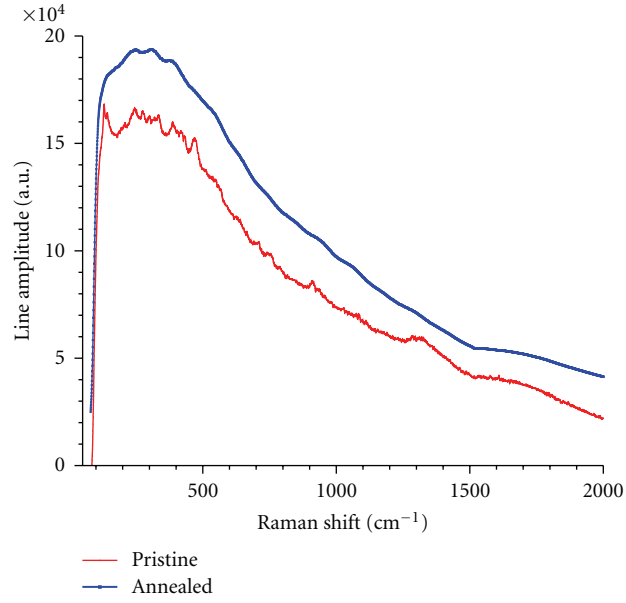

FIGURE 13: The Raman spectrum of pristine halloysite (narrow line) and of the halloysite annealed for 30 minutes at 250°C.

The Raman lines of halloysite are broad, as the experimental spectra are a convolution of spectra corresponding to molecules with various degrees of hydration. TGA data suggested that in average each two molecules of halloysite contain one molecule of water (or in other words there is one molecule of halloysite 10 A to every 4 molecules of halloysite 7 A). The existing literature suggests that the Young modulus of halloysite is three times smaller than the Young modulus of carbon nanotubes. For the same applied stress, the estimated strain should be three times larger than in carbon nanotubes. Hence, larger Raman shifts were expected in iPPH nanocomposites than in iPP-VGCNF composites. By comparing the Raman shifts reported here to the Raman shifts noticed in our previous study of iPP-VGCNF [11], it is

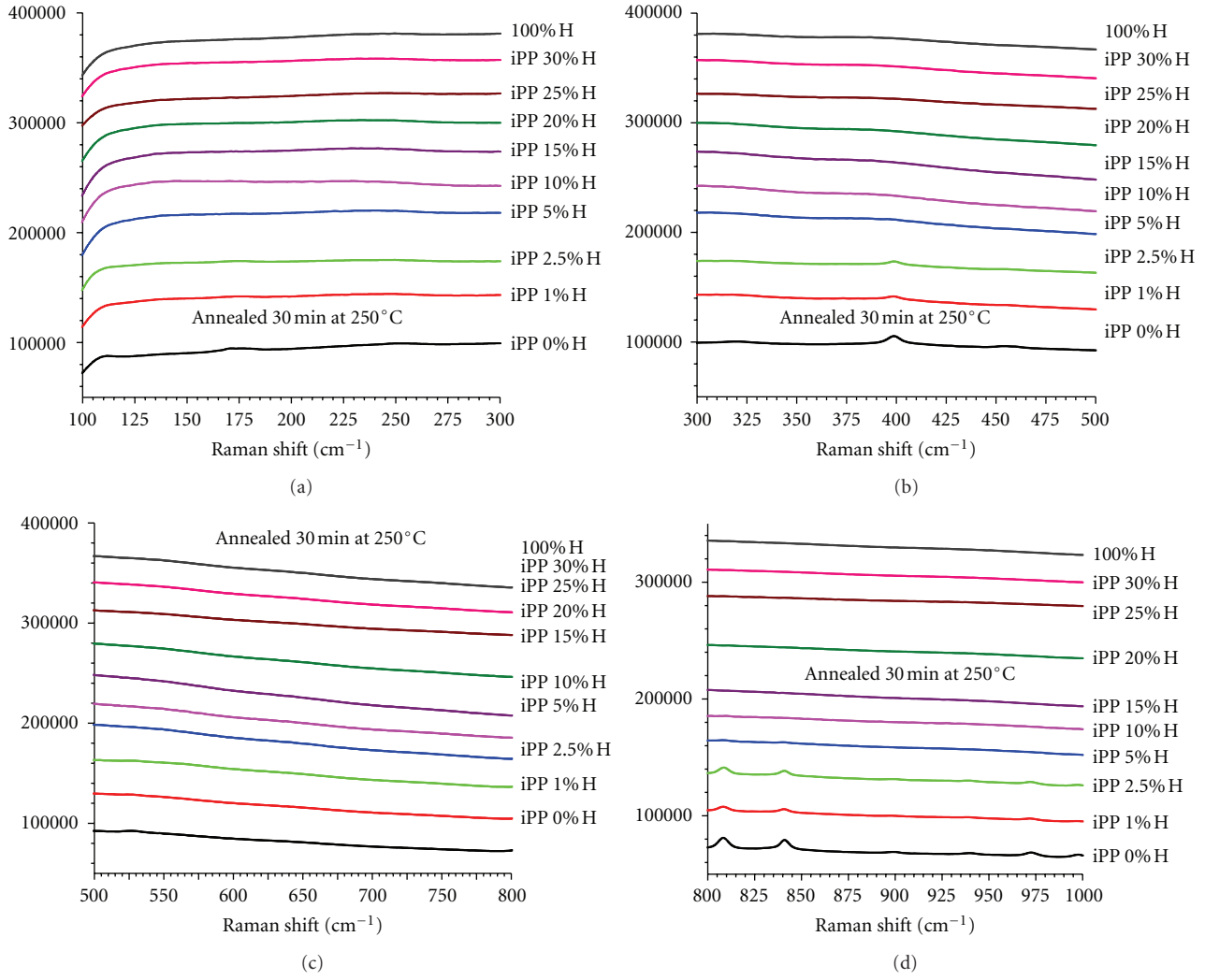

Figure 14: The Raman spectra of iPPH nanocomposites annealed at 250° for 30 minutes.

concluded that the shifts of the Raman peaks as a function of filler's concentration are weaker for halloysite (compared to VGCNF), and consequently the stress transfer between the polymeric matrix (same iPP) and the nanofiller is less efficient in the case of halloysite.

The experimental data are qualitatively analogous with the iPP-VGCNF nanocomposites; the nanofiller broadens and decreases the intensity of the Raman lines assigned to the polymeric matrix (iPP). However, due to the fact the nanofiller does not exhibit narrow and strong Raman lines, the analysis was also focused on the polymeric matrix. A detailed analysis of the modifications of the regularity band associated to the polymeric matrix is presented. The analysis of Raman lines indicates that the polymeric matrix becomes less crystalline upon the loading with halloysite and that the nanofiller is experiencing a weak dehydration upon dispersion within the polymeric matrix, probably due to the thermal processing. Raman spectroscopy failed to substantiate the growth of a gamma iPP phase due to the loading of isotactic polypropylene with halloysite as reported in [14]. In conclusion, in iPP the loading with halloysite drops the isotacticity and decreases the degree of crystallinity, in contrast with the data reported in [14]. The drop of the isotacticity of iPP as the concentration of H is increased demonstrates interactions between the polymeric matrix and the halloysite nanotubes. As discussed previously, these interactions are weaker than in iPP-VGCNF nanocomposite. Further Differential Scanning Calorimetry and Wide Angle X-Ray Scattering experiments are in course to address the crystallinity and the crystallization of these nanocomposites.

Acknowledgments

This work was supported by the National Science Foundation under DMR Grant no. 0934157 (PREM—The University of Texas-Pan American (UTPA)/University of Minnesota—Science and Engineering of Polymeric and Nanoparticle-Based Materials for Electronic and Structural Applications).

References

[1] V. Chirila, G. Marginean, T. Iclanzan, C. Merino, and W. Brandl, "Method for modifying mechanical properties of carbon nano-fiber polymeric composites," *Journal of Thermoplastic Composite Materials*, vol. 20, no. 3, pp. 277–289, 2007.

[2] K. Suzuki and S. Nomura, "On elastic properties of single-walled carbon nanotubes as composite reinforcing fillers," *Journal of Composite Materials*, vol. 41, no. 9, pp. 1123–1135, 2007.

[3] K. T. Lau, M. Chipara, H. Y. Ling, and D. Hui, "On the effective elastic moduli of carbon nanotubes for nanocomposite structures," *Composites B*, vol. 35, no. 2, pp. 95–101, 2004.

[4] F. Hussain, M. Hojjati, M. Okamoto, and R. E. Gorga, "Review article: polymer-matrix nanocomposites, processing, manufacturing, and application: an overview," *Journal of Composite Materials*, vol. 40, no. 17, pp. 1511–1575, 2006.

[5] A. Allaoui, S. V. Hoa, and M. D. Pugh, "The electronic transport properties and microstructure of carbon nanofiber/epoxy composites," *Composites Science and Technology*, vol. 68, no. 2, pp. 410–416, 2008.

[6] J. Bernholc, D. Brenner, M. Buongiorno Nardelli, V. Meunier, and C. Roland, "Mechanical and electrical properties of nanotubes," *Annual Review of Materials Science*, vol. 32, pp. 347–375, 2002.

[7] J. Li and J. K. Kim, "Percolation threshold of conducting polymer composites containing 3D randomly distributed graphite nanoplatelets," *Composites Science and Technology*, vol. 67, no. 10, pp. 2114–2120, 2007.

[8] N. Li, Y. Huang, F. Du et al., "Electromagnetic Interference (EMI) shielding of single-walled carbon nanotube epoxy composites," *Nano Letters*, vol. 6, no. 6, pp. 1141–1145, 2006.

[9] A. R. Bhattacharyya, T. V. Sreekumar, T. Liu et al., "Crystallization and orientation studies in polypropylene/single wall carbon nanotube composite," *Polymer*, vol. 44, no. 8, pp. 2373–2377, 2003.

[10] E. Logakis, E. Pollatos, C. Pandis et al., "Structure-property relationships in isotactic polypropylene/multi-walled carbon nanotubes nanocomposites," *Composites Science and Technology*, vol. 70, no. 2, pp. 328–335, 2010.

[11] C. Mircea, J. R. Villarreal, M. D. Chipara, K. Lozano, A. C. Chipara, and D. J. Sellmyer, "Spectroscopic investigations on polypropylene-carbon nanofiber composites. I. Raman and electron spin resonance spectroscopy," *Journal of Polymer Science B*, vol. 47, no. 17, pp. 1644–1652, 2009.

[12] M. D. Chipara, K. Lozano, A. Hernandez, and M. Chipara, "TGA analysis of polypropylene-carbon nanofibers composites," *Polymer Degradation and Stability*, vol. 93, no. 4, pp. 871–876, 2008.

[13] M. Chipara, J. Hamilton, A. C. Chipara, T. George, D. M. Chipara, E. E. Ibrahim et al., "Fourier transform infrared spectroscopy and wide-angle X-ray scattering: investigations on polypropylene—vapor-grown carbon nanofiber composites," *Journal of Applied Polymer Science*, vol. 125, no. 1, pp. 353–360, 2012.

[14] M. Du, B. Guo, and D. Jia, "Newly emerging applications of halloysite nanotubes: a review," *Polymer International*, vol. 59, no. 5, pp. 574–582, 2010.

[15] Y. Tang, S. Deng, L. Ye et al., "Effects of unfolded and intercalated halloysites on mechanical properties of halloysite-epoxy nanocomposites," *Composites A*, vol. 42, no. 4, pp. 345–354, 2011.

[16] E. Horváth, J. Kristóf, R. Kurdi, É. Makó, and V. Khunová, "Study of urea intercalation into halloysite by thermoanalytical and spectroscopic techniques," *Journal of Thermal Analysis and Calorimetry*, vol. 105, no. 1, pp. 53–59, 2011.

[17] B. Lecouvet, M. Sclavons, S. Bourbigot, J. Devaux, and C. Bailly, "Water-assisted extrusion as a novel processing route to prepare polypropylene/halloysite nanotube nanocomposites: structure and properties," *Polymer*, vol. 52, no. 19, pp. 4284–4295, 2011.

[18] L. Guimarães, A. N. Enyashin, G. Seifert, and H. A. Duarte, "Structural, electronic, and mechanical properties of single-walled halloysite nanotube models," *Journal of Physical Chemistry C*, vol. 114, no. 26, pp. 11358–11363, 2010.

[19] K. H. Michaelian, S. L. Zhang, S. Yariv, and I. Lapides, "Low-frequency Raman spectra of kaolinite/alkali halide complexes," *Applied Clay Science*, vol. 13, no. 4, pp. 233–243, 1998.

[20] S. D. M. Brown, A. Jorio, P. Corio et al., "Origin of the Breit-Wigner-Fano lineshape of the tangential G-band feature of metallic carbon nanotubes," *Physical Review B*, vol. 63, no. 15, Article ID 155414, pp. 1554141–1554148, 2001.

[21] R. L. Frost and H. F. Shurvell, "Raman microprobe spectroscopy of halloysite," *Clays and Clay Minerals*, vol. 45, no. 1, pp. 68–72, 1997.

[22] R. L. Frost, T. H. Tran, and J. Kristof, "FT-Raman spectroscopy of the lattice region of kaolinite and its intercalates," *Vibrational Spectroscopy*, vol. 13, no. 2, pp. 175–186, 1997.

[23] R. L. Frost, "Fourier transform Raman spectroscopy of kaolinite, dickite and halloysite," *Clays and Clay Minerals*, vol. 43, no. 2, pp. 191–195, 1995.

[24] J. T. Kloprogge and R. L. Frost, "Raman microprobe spectroscopy of hydrated halloysite from a neogene cryptokarst from Southern Belgium," *Journal of Raman Spectroscopy*, vol. 30, no. 12, pp. 1079–1085, 1999.

[25] M. Arruebarrena de Báez, P. J. Hendra, and M. Judkins, "The Raman spectra of oriented isotactic polypropylene," *Spectrochimica Acta A*, vol. 51, no. 12, pp. 2117–2124, 1995.

[26] T. Hahn, W. Suen, S. Kang, S. L. Hsu, H. D. Stidham, and A. R. Siedle, "An analysis of the Raman spectrum of syndiotactic polypropylene. 1. Conformational defects," *Polymer*, vol. 42, no. 13, pp. 5813–5822, 2001.

[27] T. Sundell, H. Fagerholm, and H. Crozier, "Isotacticity determination of polypropylene using FT-Raman spectroscopy," *Polymer*, vol. 37, no. 15, pp. 3227–3231, 1996.

[28] R. M. Khafagy, "In situ FT-Raman spectroscopic study of the conformational changes occurring in isotactic polypropylene during its melting and crystallization processes," *Journal of Polymer Science B*, vol. 44, no. 15, pp. 2173–2182, 2006.

[29] V. M. Hallmark, S. P. Bohan, H. L. Strauss, and R. G. Snyder, "Analysis of the low-frequency isotropic Raman spectrum of molten isotactic polypropylene," *Macromolecules*, vol. 24, no. 14, pp. 4025–4032, 1991.

[30] D. E. Gen, K. A. Prokhorov, G. Y. Nikolaeva et al., "Raman spectra of various polymorphs of isotactic polypropylene," *Laser Physics*, vol. 21, no. 1, pp. 125–129, 2011.